2019-24-0017 Published 09 Sep 2019

Cylinder Pressure Based Method for In-Cycle Pilot Misfire Detection

Carlos Jorques Moreno and Ola Stenlåås Scania CV AB

Per Tunestål Lund University

Citation: Jorques Moreno, C., Stenlåås, O., and Tunestål, P., "Cylinder Pressure Based Method for In-Cycle Pilot Misfire Detection," *SAE Int. J. Advances & Curr. Prac. in Mobility* 2(2):488-502, 2020, doi:10.4271/2019-24-0017.

This article was presented at the 14th International Conference on Engines & Vehicles, Capri, Italy, September 15-19, 2019.

Abstract

For the reduction of emissions and combustion noise in an internal combustion diesel engine, multiple injections are normally used. A pilot injection reduces the ignition delay of the main injection and hence the combustion noise. However, normal variations of the operating conditions, component tolerances, and aging may result in the lack of combustion i.e. pilot misfire. The result is a lower indicated thermal efficiency, higher emissions, and louder combustion noise. Closed-loop combustion control techniques aim to monitor in real-time these variations and act accordingly to counteract their effect. To ensure the in-cycle controllability of the main injection, the misfire diagnosis must be performed before the start of the main injection. This paper focuses on the development and evaluation of in-cycle algorithms for the pilot misfire detection.

Based on in-cylinder pressure measurements, different approaches to the design of the detectors are compared. For non-adaptive methods, a constant threshold, direct misfire probability, and posterior misfire probability detectors are investigated. For adaptive methods, an adaptive threshold update is suggested, an adaptation of the predictive stochastic models and a sensor fusion of them is proposed to increase the detection performance.

A Scania D13 engine is used to perform the experiments under different operating conditions. The effectiveness of the algorithms is tested for different engine speeds, rail pressures, injection durations, starts of injection, EGR levels, and fuels. The results show that the observability of in-cycle pilot misfire depends on the operating conditions, and its detection can be performed successfully before the start of the main injection. With a maximum in-cycle pilot misfire observability of 98.5%, a maximum successful detection ratio of about 96% can be reached with the proposed in-cycle pilot misfire detectors. The algorithms are therefore suitable for in-cycle closed-loop combustion control feedback. By including cycle-to-cycle adaptation, the detection performance and robustness are improved significantly. The limitations are directly related to the signal-to-noise ratio of each operating condition.

Introduction

Pilot injections are commonly used in heavy-duty diesel engines to reduce emissions and noise under legislation limits. This is possible with the aid of fast common-rail injectors that allow multiple injections within the same cycle. The different operating conditions, with special attention to cold start, and variation of the fuel properties, may result in the misfire of the pilot injection. Furthermore, the production tolerances between injectors, aging, rail pressure oscillations, and normal variations increase the uncertainty of the injected fuel mass for a constant on-time. These variations further increase the uncertainty of pilot misfire [1].

Pilot misfire has a significant effect on the shape of the main injection heat release [2]. Namely, the ignition delay increases, raising the peak of the initial premixed combustion. The fast, premixed combustion results in a lower indicated thermal efficiency, increased combustion noise and pollutant emissions. The effect of pilot misfire is dependent on operating conditions [2], and despite it has a less significant effect on the heat release shape at high loads, it still has a significant effect on emissions. Furthermore, pilot misfire is important to be diagnosed in cases where the lack of its combustion may result also in the lack of the main combustion if it is not adjusted, such as at cold starts of partially-premixed combustion concepts [3]. Typically, the risk of pilot misfire is reduced by increasing the nominal pilot mass. However, this also reduces the nominal indicated thermal efficiency. By in-cylinder pressure measurements, real-time feedback of the combustion is obtained. Closed-loop combustion control algorithms use real-time information to re-compute the optimal main injection. This reduces the effect of the pilot combustion variations on the cycle performance [4], while still having a reduced nominal pilot mass.

Several methods for misfire diagnosis and identification are found in the literature as is legislated by OBD-II. A minimum performance is required. For example, misfire must be diagnosed in one or more cylinders when it exceeds 5%, evaluated

© 2019 Scania CV AB, Carlos Jorques Moreno, Ola Stenlåås, Per Tunestål. Published by SAE International. This Open Access article is published under the terms of the Creative Commons Attribution License (http://creativecommons.org/licenses/by/4.0/), which permits distribution, and reproduction in any medium, provided that the original author(s) and the source are credited.

© 2019 Scania CV AB, Carlos Jorques Moreno, Ola Stenlåås, Per Tunestål.

in 1000 cycles, according to the latest CARB legislation for heavy-duty engines [5]. The methods are based on available measurement variables, see [6] for an overview. Examples of the different measured variables are the instantaneous engine speed [7, 8, 9], further improved with the aid of model-based methods [10], or sliding-mode observers [11], to name some of the multiple used techniques. Also, sound measurements by knock sensors [12,13] or accelerometers [14,15] are used. For spark-ignition engines where the spark-plug can be used as a sensor, the ion-current signal [16,17] is also proposed for misfire diagnosis. For improved robustness, even combinations of multiple signals are suggested [18]. In-cylinder pressure measurements have also been used for the misfire diagnosis [19]. Very few methods to identify misfire of multiple injections were found. An exception is [20] where the ion-current sensor is used to detect the combustion of the pilot with a simple threshold. However, this makes it more sensitive to measurement noise, in the cases of short pilot on-times and short pilot-main SOI separations, and less robust to changing operating conditions.

The novelty of this paper is its focus on how pilot misfire can be robustly diagnosed in-cycle, i.e. before the main start of injection. For that purpose, the combustion information is obtained from fast in-cylinder pressure measurements. The aim is its use for in-cycle closed-loop combustion control. The study presents a comparison of different detectors design. The methods are based on direct thresholds as the decision rule and a Bayesian approach. Two approaches for the stochastic characterization of the combustion variables are studied. The first one uses direct modeling of the conditional posterior probabilities. The second one uses the Bayes theorem to compute the posterior probabilities based on predictive stochastic models. The methods are extended by suggested adaptation schemes. The performance, robustness, and sensitivity of the methods are analyzed.

In this research, the necessary information for an effective and robust diagnosis of the pilot misfire in-cycle, and the required CAD-frame to obtain that information are investigated. The off-line calibration effort and its on-line adaptation, and how the combination of different signals can improve the diagnosis performance are also considered. Finally, the robustness and sensitivity of the methods to the operating conditions and fuel type are studied.

Experimental Setup

A modified Scania D13 six-cylinder engine with common rail was used for the experiments. The geometrical specifications of the engine are listed in Table 1:

TABLE 1 Engine geometrical specifications.

Parameter	Value
Cylinder number	6
Displaced volume	12.74 L
Stroke	160 mm
Bore	130 mm
Compression ratio	18:1
Number of Valves	4
Intake Valve Closing timing (IVC)	-151 CAD ATDC
Exhaust Valve Opening timing (EVO)	146 CAD ATDC

© 2019 Scania CV AB, Carlos Jorques Moreno, Ola Stenlåås, Per Tunestål.

An illustration of the engine setup is in Figure 1:

FIGURE 1 Experimental setup diagram

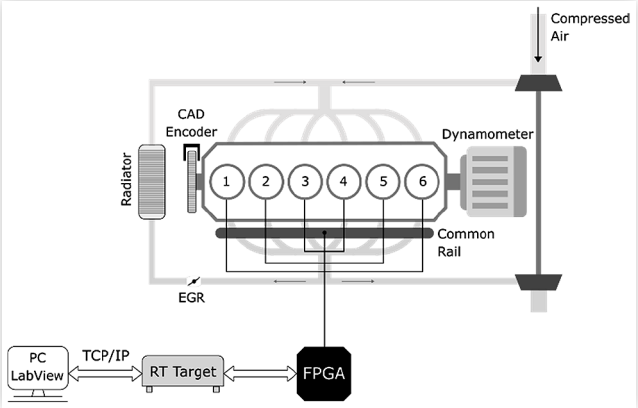

© 2019 Scania CV AB, Carlos Jorques Moreno, Ola Stenlåås, Per Tunestål.

In-cylinder Kistler 7061B relative pressure piezo-electric transducers were available at each of the cylinders. These sensors were water cooled for improved accuracy. The rail pressure was measured by a production piezo-resistive transducer. Both, the in-cylinder pressure and the rail pressure were synchronized with the crank angle encoder signal, sampled by Leine-Linde encoder with 0.2 CAD resolution. For the intake and exhaust manifold, the absolute pressure was measured by Keller PAA-23S pressure sensors. The inlet and exhaust manifold temperature were measured by K-type thermocouples. The brake torque after the fly-wheel was measured by an HBM T40B torque sensor. The exhaust gas emissions were measured by a Horiba MEXA-9100E. For the control of the EGR, two regulated ball valves controlled the low-pressure and high-pressure routes. The engine speed was controlled by a 355kW AC motor used as dynamometer and brake.

For the operation of the engine, the real-time control was distributed in three processors. A Field Programmable Gate Array (FPGA) was used for the fast sampling and control of the injection. The FPGA used for this project was a NI FPGA module NI PXI-7854/7854 R, with a Virtex 5-LX110/LX30 FPGA. The real-time control was implemented in a PXI chassis (NI PXIe-8135 2.3 GHz quad-core processor) and executed at 100Hz. The real-time target communicated with a PC via the TCP/IP protocol. A dedicated LabView Software was implemented for the interface with the user.

Design of Experiments

The most significant variables on the pilot misfire are the pilot mass and the in-cylinder pressure at the start of injection. Therefore, a full combination of pilot injection on-times and SOI were swept for three rail pressures, three engine speeds, and three EGR levels. Additionally, this was repeated for three different fuel types: conventional diesel fuel, hydrogenated vegetable oil (HVO) and Rapeseed Methyl Esters (RME). The values are in Table 2:

© 2019 Scania CV AB, Carlos Jorques Moreno, Ola Stenlåås, Per Tunestål.

TABLE 2 Variables and values of central matrix design

Variable	Value
On-time	0.2 ms to 0.4 ms in steps of 0.02 ms
SOI	-38 CAD to -10 CAD in steps of 2 CAD
Rail Pressure	800, 1200, 1600 bar
Engine Speed	800, 1200, 1600 RPM
EGR	0, 10, 20, 30%
Fuel	RME, HVO, diesel

© 2019 Scania CV AB, Carlos Jorques Moreno, Ola Stenlåås, Per Tunestål.

To complement the intermediate values while keeping the total number of experiments to a feasible number, the previous points were extended to a limited number of on-times and SOI. These on-times were selected to be within the transition from pilot misfire to pilot combustion. The intermediate values are summarized in Table 3:

TABLE 3 Variables and complementary intermediate values of central matrix design

Variable	Value
On-time	0.24 ms to 0.34 ms in steps of 0.02 ms
SOI	-38 CAD to -10 CAD in steps of 4 CAD
Rail Pressure	1000, 1400 bar
Engine Speed	1000, 1400 RPM
Fuel	RME, HVO, diesel

© 2019 Scania CV AB, Carlos Jorques Moreno, Ola Stenlåås, Per Tunestål.

Pilot Misfire

The pilot combustion has the effect of reducing the main ignition delay and its premixed peak. The decrease or non-occurrence of combustion, i.e. pilot misfire, increases the premixed peak of the main combustion, resulting in a decreased indicated thermal efficiency. Consequently, pilot misfire is defined in this work as the lack of enough pilot combustion resulting in an increase of the premixed peak of the main injection's combustion. The above definition of pilot misfire can be extended, without loss of generality, to any injection and its effect on what follows. Implicitly, the lack of perceived pilot heat release, due to locally bounded combustion or small cylinder pressure change, does not imply its classification as misfire. The other situation may also occur when despite a positive magnitude of the pilot heat release rate, there is pilot misfire. The in-cycle pilot misfire detector can be understood as a predictor stating whether the measured pilot heat release will be enough to reduce the premixed peak of the main combustion or not. Some of the challenges for the in-cycle pilot misfire detection are exemplified in Figure 2:

FIGURE 2 Comparison of the heat release between fire and misfire cases. In the upper plot (a), the lack of pilot heat release despite apparent pilot combustion is compared to single injection. The middle plot (b) shows when similar pilot HR has different misfire classification. In the lower plot (c), the effect of high engine speeds (1600RPM) is illustrated for a single injection (black) and pilot-main injections (red). The oscillations on the heat release rate due to the higher turbulence result in a smaller difference on the premixed peak of the main heat release rate for the fire and misfire cases.

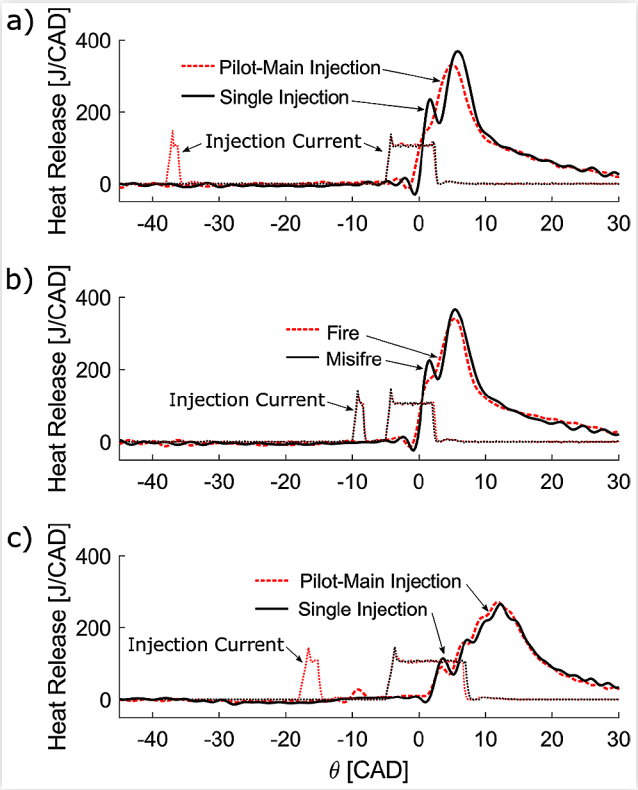

© 2019 Scania CV AB, Carlos Jorques Moreno, Ola Stenlåås, Per Tunestål.

From the adopted definition of pilot misfire, the whole cycle is used to classify it as misfire or not. This is done by measuring the magnitude of the premixed peak of the main injection's heat release rate. Due to oscillations on the trace at high engine speeds, the threshold to identify a pilot misfire needs to be adapted to the engine operation to avoid a wrong classification. To do that, the single injection case is used for reference to the calibration of the expected main heat release premixed peak subject to pilot misfire. A long pilot on-time and late injection is used for the reference calibration of the main's heat release premixed peak subject to pilot combustion. By comparing how similar the measured main premixed heat release magnitude is to each of the cases, the cycle is classified as a misfire or combustion.

In-Cycle Pilot Misfire Detection

The different available variables to perform the in-cycle pilot misfire detection, the in-cycle pilot misfire observability, the

© 2019 Scania CV AB, Carlos Jorques Moreno, Ola Stenlåås, Per Tunestål.

detection methods and the models used are presented in this section.

Available Measured and Estimated Variables

For the in-cycle diagnosis of the pilot misfire, different measured and estimated variables are available. The directly measured variable is the in-cylinder pressure. From it, the estimated variables are the heat release rate (HR), the accumulated heat release (AHR) and the pressure rise over the estimated motoring trace. For simplicity in the text, it will further be referred to as pressure rise. This last one has the advantage compared to the AHR of requiring less filtering and processing, as the pressure derivative is not required. From the in-cylinder pressure trace, its frequency content can also be used. However, during the analysis of the data, it was observed that the signal-to-noise ratio is too low for robust diagnosis of pilot misfire. The performance of the pilot misfire detection using the other variables and their combination will be compared.

In-Cycle Pilot Misfire Observability

The previous examples in Figure 2 illustrate how challenging the in-cycle pilot misfire detection can be. In fact, some operating points may result in insufficient observability with the measured variables. This means that there is not enough correlation between the measured variables and the pilot misfire. Hence, it cannot be predicted before the main combustion. To address the in-cycle pilot misfire observability, an optimal threshold for each of the measured and estimated variables was derived, individually for each operating point. Optimality is defined as the fraction of correctly diagnosed cycles. The combined optimal misfire observability is obtained by deciding the correct diagnosis if any of the variables detected it correctly. This can not be done on-line and is only used for reference.

Optimal Misfire Detector

In this work, a Bayesian decision approach was taken to minimize the average detection error probability. This is equivalent to maximizing the detection performance, measured as the fraction of correctly detected pilot combustion or misfire. The decision rule to optimize the average detection error, where x is the measured variable, is:

$$decide\ misfire: P(misfire|x) > P(fire|x) \tag{1}$$

Two approaches to obtain the probabilities are studied. The first one is the direct modeling of the misfire probability for a given measured value of each variable. In the second approach, the value of each variable is predicted together with its uncertainty. By applying Bayes rule, the posterior probability of pilot combustion and misfire are computed. The first approach provides a systematic method for having a variable threshold on the measured variables with the operating conditions. The second approach simplifies how the probability distributions are updated by cycle-to-cycle feedback and how the different sensors' information is combined. The stochastic models to obtain the probabilities are described in the following section.

As a reference to compare how the Bayesian approach can improve the detection performance, another simple detection method is used. The method uses a direct threshold, γ, on the measured variables, x:

$$decide\ misfire: x > \gamma \tag{2}$$

For the threshold calibration, it was swept over the whole data set. The value resulting in the best detection performance, measured as the successful detection ratio, was used as a reference for comparison with the other algorithms. The optimal threshold is a trade-off between better combustion detection against better misfire detection, which depends on the signal-to-noise ratio.

Stochastic Models

Probability Distribution models

In this approach, the misfire probability for a given value of each measured variable is modeled directly.

Pilot Heat Release Magnitude The stochastic model must describe the probability of having a misfire event given a measured heat release magnitude of the pilot. Intuitively, this could be described with a degenerated distribution, so that pilot combustion is decided whenever the magnitude of the pilot heat release is positive. However, the measurement noise of the heat release and the normal variations of the combustion process (see Figure 2) suggest that a normal distribution is more accurate to describe the probability of pilot misfire for a given measured heat release magnitude. This was the model adopted.

There is a phenomenon observed before the main SOC when an additional oscillation of the filtered heat release trace is obtained, see the middle plot (b) in Figure 2. For an expected pilot combustion before the main SOI, this is not an issue. However, if the pilot-main separation is too short, these oscillations could be confounded as heat release from the pilot. Hence, to increase the detection performance, the model uses the pilot-main start of injection separation ($\Delta\theta_{pilot-main}$) to increase the expected pilot HR magnitude linearly. The final model is:

$$P(misfire|HR) \sim \mathrm{N}\left(HR|\,\mu_{HR}, \sigma^2_{HR}\right) \tag{3}$$

$$\mu_{HR} = \mu_0 + k_{\mu a} e^{-k_{\mu b} \cdot \Delta\theta_{pilot-main}} \tag{4}$$

$$\sigma^2_{HR} = k_{\sigma a} + k_{\sigma b} \cdot \Delta\theta_{pilot-main} \tag{5}$$

© 2019 Scania CV AB, Carlos Jorques Moreno, Ola Stenlåås, Per Tunestål.

This model is used for all the operating conditions and it was calibrated from the data points in Table 2. The result of the model is plotted in Figure 3:

FIGURE 3 Pilot misfire probability as a function of the heat release magnitude, under the operating conditions of Table 2, for different pilot SOI.

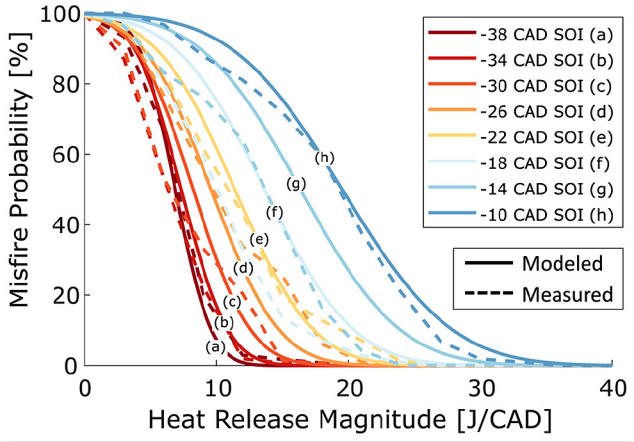

© 2019 Scania CV AB, Carlos Jorques Moreno, Ola Stenlåås, Per Tunestål.

Pilot Accumulated Heat Release The accumulated heat release will further increase the robustness of the detection algorithm, especially for the cases when the pilot heat release magnitude can be confounded with noise. The misfire probability is modeled as a normal distribution whose mean and variance are functions of the pilot start of injection. The model is:

$$P(misfire|AHR) \sim N\left(AHR|\,\mu_{AHR},\sigma^2_{AHR}\right) \tag{6}$$

$$\mu_{AHR} = \mu_0 + k_{\mu a}\cdot\left(\theta_{SOI}-\theta_0\right)^2 \tag{7}$$

$$\sigma^2_{AHR} = \sigma_0 + k_{\sigma a}\cdot e^{-k_{\sigma b}\theta_{SOI}} \tag{8}$$

The results of the model are plotted in Figure 4:

FIGURE 4 Pilot misfire probability as a function of the accumulated heat release, under the operating conditions of Table 2, for different pilot SOI.

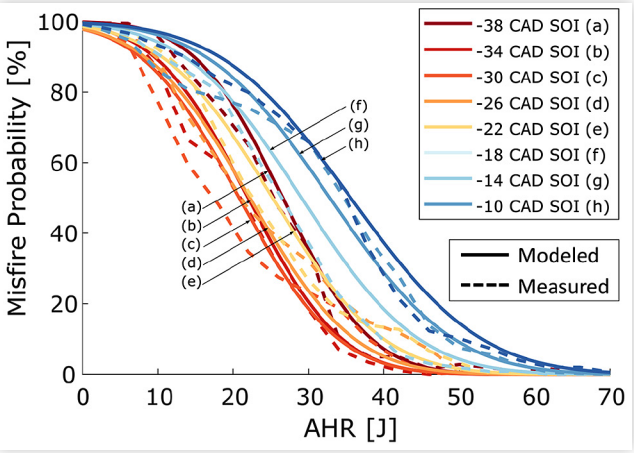

© 2019 Scania CV AB, Carlos Jorques Moreno, Ola Stenlåås, Per Tunestål.

Pressure Rise over Motoring The probability model of the pressure rise is modeled as a normal distribution with variable mean and standard deviation, which are functions of the pilot start of injection:

$$P(misfire|\Delta P) \sim \mathrm{N}\left(\Delta P|\,\mu_{\Delta P},\sigma^2_{\Delta P}\right) \tag{9}$$

$$\mu_{\Delta P} = \mu_0 + k_{\mu a}\cdot\theta_{SOI} \tag{10}$$

$$\sigma^2_{\Delta P} = \sigma_0 + k_{\sigma a}\cdot\left(\theta_{SOI}-\theta_0\right)^2 \tag{11}$$

The result is plotted in Figure 5:

FIGURE 5 Pilot misfire probability as a function of the pressure rise over motoring, under the operating conditions of Table 2, for different pilot SOI.

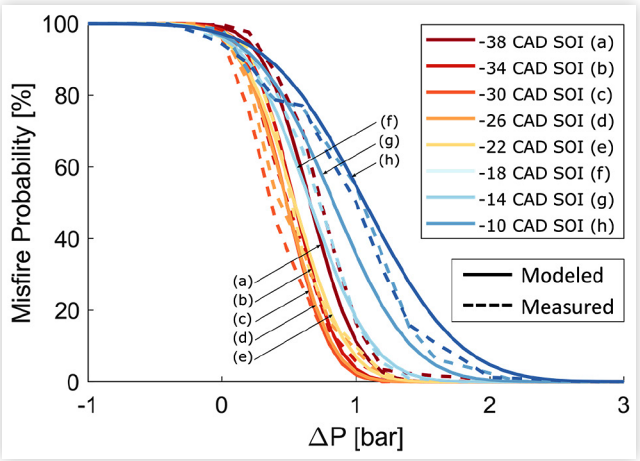

© 2019 Scania CV AB, Carlos Jorques Moreno, Ola Stenlåås, Per Tunestål.

Predictive Stochastic Models

In this approach, the pilot heat release magnitude, its CAD position, the pilot accumulated heat release and the pressure rise over motoring are modeled. Their value and uncertainty are predicted under the two hypotheses, pilot combustion, and pilot misfire. The posterior probability is then computed by the Bayes rule:

$$P(misfire|x) = \frac{P(x|misfire)\,P(misfire)}{P(x)} \tag{12}$$

Where x is the measured variable. The misfire probability is the prior probability of obtaining pilot misfire when no more information but the injected pilot mass and the SOI are known. The prior probability of obtaining a measured value of x is computed via the law of total probability:

$$P(x) = P(x|misfire)\,P(misfire) + P(x|fire)\left(1-P(misfire)\right) \tag{13}$$

The required models are hence $P(x|\,misfire)$, i.e. the distribution of the noise in a given variable, and $P(x|\,fire)$ i.e. the expected value and its uncertainty. The advantage with this approach is that the predictions can easily be adapted for an improved in-cycle detection performance. This will be discussed in the next section.

© 2019 Scania CV AB, Carlos Jorques Moreno, Ola Stenlåås, Per Tunestål.

Prior Pilot Misfire Probability The prior probability describes the expected risk of pilot misfire for a given operating condition before any additional information is available. It is therefore modeled as a normal distribution whose mean and standard deviation are functions of the start of injection and the off-line calibrated pilot mass i.e. injector map:

$$P(misfire) \sim N\left(m_{pilot};\mu_{misfire},\sigma^2_{misfire}\right) \tag{14}$$

$$\mu_{misfire} = \mu_0 + k_\mu \cdot e^{-\beta\theta_{SOI}} \tag{15}$$

$$\sigma^2_{misfire} = \sigma_0 + k_\sigma \cdot \left(\theta_{SOI} - \theta_0\right)^2 \tag{16}$$

The result is plotted in Figure 6:

FIGURE 6 Pilot misfire prior probability model as a function of the pilot mass, under the operating conditions of Table 2, for different pilot SOI.

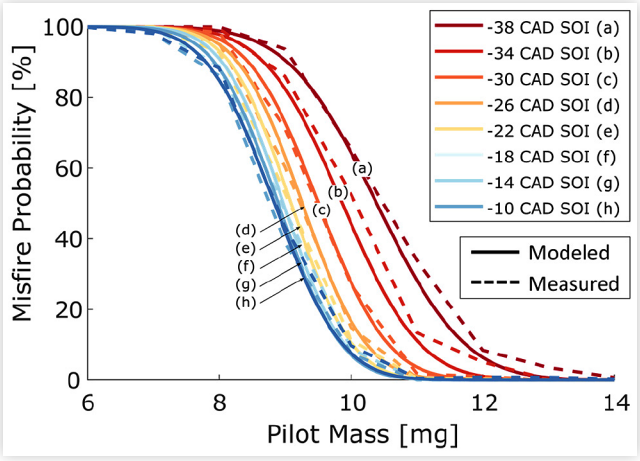

© 2019 Scania CV AB, Carlos Jorques Moreno, Ola Stenlåås, Per Tunestål.

The uncertainty of the off-line calibrated injectors map is included in this model, which increases the total uncertainty of pilot misfire. If the injector were individually calibrated on-line, the uncertainty could be reduced for better detection performance.

Ignition Delay The ignition delay prediction has two applications. The first is to locate the range where to measure the magnitude of the pilot heat release. This reduces the risk of confounding oscillations with the actual heat release magnitude. The second application is its use in the pilot heat release magnitude model. The ignition delay is related to the mixing of the fuel and hence how much is available at the time of auto-ignition.

Rather than having a highly accurate and complex model, a simple model to describe the position of the start of the pilot combustion under a few crank angle degrees uncertainty is sufficient. A simple model that proved to describe adequately the ignition delay for the small pilot masses that are investigated is:

$$\tau_{ID} = \left(\tau_0 + k \cdot e^{-a \cdot P_{SOI}}\right) \tag{17}$$

$$\Delta\theta_{ID} = \frac{1000}{60 n_{eng}} \tau_{ID} \tag{18}$$

The uncertainty of the model is described as a normal distribution with a constant standard deviation over the whole operation range, in the CAD domain. The stochastic model is:

$$P(\theta_{SOC}|fire) \sim N\left(\theta_{SOI} + \Delta\theta_{ID}, \sigma^2_{ID}\right) \tag{19}$$

The ignition delay is then used to estimate the position of the maximum pilot heat release, the accumulated heat release and the pressure rise over the motoring. From the results in [1], the maximum pilot heat release is placed 2 CAD after the pilot SOC. To have a robust evaluation of the accumulated heat release and the pressure rise over motoring, they are evaluated another 2 CAD after the pilot heat release magnitude. Hence, $\Delta\theta_{HR} = 2\ CAD$, $\Delta\theta_{AHR} = 4\ CAD$ and $\Delta\theta_{PD} = 4\ CAD$.

The result of the CAD at the maximum pilot heat release is plotted in Figure 7 for the whole range of experiments. The three-standard deviation lines are included to represent the uncertainty of the model.

Pilot Heat Release Magnitude The magnitude of the pilot heat release is modeled as a function of the injection on-time, rail pressure and the in-cylinder pressure at the start of injection. The first two define the injected pilot mass. The in-cylinder pressure is correlated with the reactivity of the mixture Additionally, the rail pressure has the effect of faster mixing and hence faster combustion, which increases the magnitude of the pilot heat release. The final model is:

$$q_{HR} = q_0 + k\exp\left(-\alpha \frac{\left(\tau_{ID} - \tau_0\right)^2}{\tau_{ID}}\right) \tag{20}$$

$$q_0 = k_{q0} + k_{q1} P_{rail} + k_{q2} t_{inj} \tag{21}$$

$$\tau_0 = k_{\tau 0} + k_{\tau 1}\left(P_{rail} - P_0\right)^2 + k_{\tau 2} t_{inj} + k_{\tau 3} P_{rail} \cdot t_{inj} \tag{22}$$

The model is empirical, and its uncertainty is modeled as a normal distribution with zero mean and a calibrated constant standard deviation. The results of the model are illustrated by the examples in Figure 8. The model of the magnitude of the heat release under misfire is a model of the expected noise and

FIGURE 7 CAD elapsed from the start of pilot injection to the position of the maximum pilot heat release, under the operating conditions of Table 2, for different engine speeds. The 3-sigma standard deviations are plotted (dotted lines) to represent the model uncertainty.

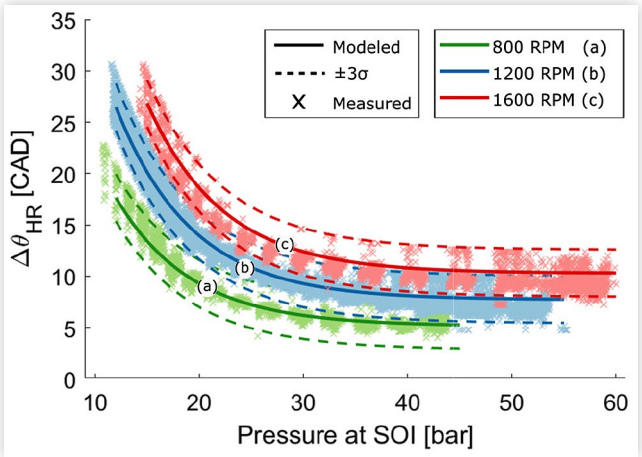

© 2019 Scania CV AB, Carlos Jorques Moreno, Ola Stenlåås, Per Tunestål.

© 2019 Scania CV AB, Carlos Jorques Moreno, Ola Stenlåås, Per Tunestål.

FIGURE 8 Pilot heat release magnitude model for different on-times at 1200 bar rail pressure (left) and different rail pressures at 0.36 ms on-time, under the operating conditions of Table 2. The 3-sigma standard deviations are plotted (dotted lines) to represent the dispersion.

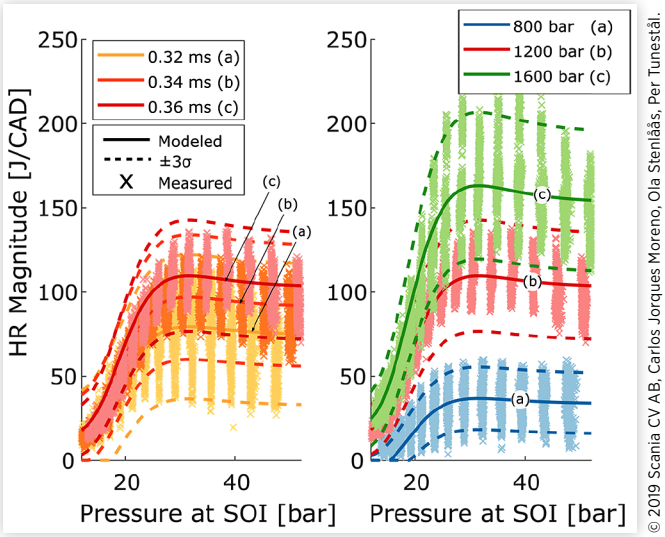

© 2019 Scania CV AB, Carlos Jorques Moreno, Ola Stenlåås, Per Tunestål.

oscillations of the heat release. It is hence modeled as a normal distribution with a calibrated constant mean and standard deviation.

Pilot Accumulated Heat Release The accumulated heat release is modeled as a linear function of the magnitude of the pilot heat release. This simple model makes use of the results in [1], where it is shown that for small pilot masses the combustion duration is constant. Hence, the accumulated heat release is approximated as proportional to the heat release magnitude. The equation describing the model is:

$$Q_{pilot} = k_{Q0} + k_{Q1} \cdot q_{HR} \tag{23}$$

The uncertainty is modeled as a normal distribution with zero mean and a calibrated constant standard deviation. The result is plotted in Figure 9:

FIGURE 9 Accumulated pilot heat release model as a function of the pilot heat release magnitude, under the operating conditions of Table 2. The 3-sigma standard deviations are plotted (dotted lines) to represent the data dispersion and model accuracy.

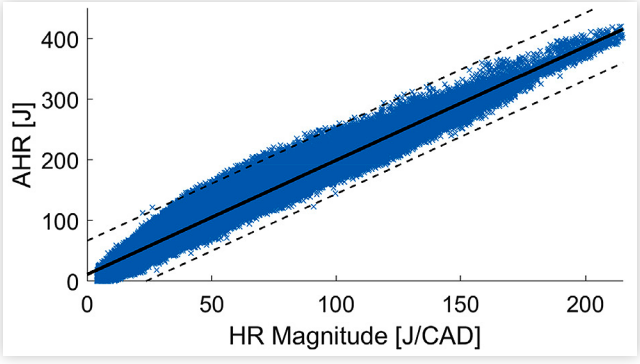

© 2019 Scania CV AB, Carlos Jorques Moreno, Ola Stenlåås, Per Tunestål.

Similar to the modeling of the magnitude of the heat release, the model for the accumulated heat release subject to pilot misfire is modeled as a normal distribution, with zero mean and a calibrated constant standard deviation.

Pressure Rise Over Motoring The pressure rise over the motoring pressure trace is directly correlated with the energy released during the combustion. The benefit in using the pressure is that only the motoring pressure needs to be estimated, but no computation of the pressure derivative is required. The model, therefore, has the same structure as the model for the accumulated heat release:

$$\Delta P = k_{p0} + k_{P1} \cdot q_{HR} \tag{24}$$

The result of the model is plot in Figure 10:

FIGURE 10 Pilot pressure rise over the motoring pressure, modeled as a function of the pilot heat release magnitude, under the operating conditions of Table 2. The 3-sigma standard deviations are plotted (dotted lines) to represent the data dispersion and model accuracy.

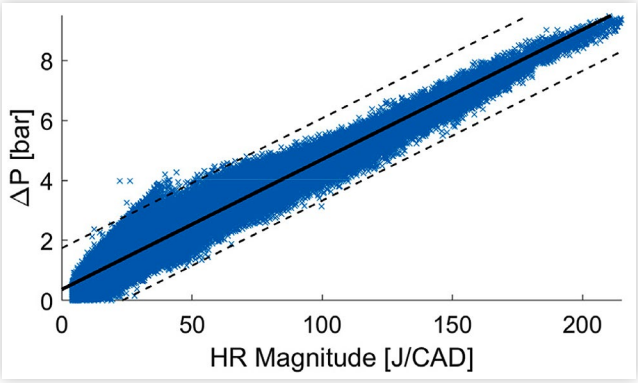

© 2019 Scania CV AB, Carlos Jorques Moreno, Ola Stenlåås, Per Tunestål.

The model for the pressure rise subject to pilot misfire is modeled as a normal distribution, with zero mean and a calibrated constant standard deviation.

Model Calibration

For the calibration of the models, enough representative data must be collected. For the direct misfire probability models, the dispersion range must be covered. This means that a wide spectrum of operating conditions is required for the stochastic characterization. Mostly, the pilot mass and SOI, but also engine speed and rail pressure are the significant variables to the misfire dispersion [1]. On the other hand, for the predictive stochastic models, a suitable design of experiments with the variables used is sufficient, which reduces the calibration effort despite the larger number of parameters. The total number of parameters of each model is summarized in Table 4, with the number of the variables for the distribution model in brackets:

© 2019 Scania CV AB, Carlos Jorques Moreno, Ola Stenlåås, Per Tunestål.

TABLE 4 Number of calibration parameters for each of the methods

	Parameters in the Probability Model	Parameters in the Predictive Stochastic model
Ignition delay	-	3+(1)
Heat release magnitude	5	12+(1)+(1)
Accumulated heat release	6	2+(1)+(1)
Pressure rise over motoring	5	2+(1)+(1)
Prior misfire probability	-	6
TOTAL	16	32

© 2019 Scania CV AB, Carlos Jorques Moreno, Ola Stenlåås, Per Tunestål.

Adaptive In-Cycle Pilot Misfire Detection

Predictive Model Adaptation

The in-cycle detection is bounded to be completed before the main start of injection. However, the information from the misfire diagnosis once the cycle is completed can be used to update the stochastic models. The adapted stochastic models are used for the pilot misfire detection of the following cycles, which will improve the performance and robustness of the algorithm.

To prove this hypothesis, a simple adaptation scheme was tested. Assuming the model error is a constant bias, it can be updated by a recursive equation:

$$e_{n+1} = (1-\alpha)e_n + \alpha(x_n - \hat{x}_n) \tag{25}$$

$$\hat{x}_n = f(u_n) + e_n \tag{26}$$

Where x_n is the measured variable, $\hat{x}_n$ is the predicted and corrected variable by the model f, using the inputs u. n is the cycle index. The adaptation gain, α, is calibrated such that the measured average error converges to zero fast enough while avoiding instability.

In the same manner, the variance can be estimated by the stream of new measurements and the corrected prediction. The recursion needs to have a forgetting factor so the estimation can be adjusted when the operating conditions are changed:

$$\sigma^2_{n+1} = (1-\alpha)\sigma^2_n + \alpha(x_n - \hat{x}_n)^2 \tag{27}$$

The adaptation gain α is calibrated considering the trade-off between a more accurate variance estimate and fast adaptation to the new operating conditions. An example of the adaptation performance of the pilot heat release magnitude is plotted in Figure 11:

FIGURE 11 Pilot heat release magnitude prediction by the model and by the adapted model. The 3-sigma standard deviations are plotted (light dotted lines) to show the uncertainty of the models. The engine was operated at 1200 RPM, 1200 bar rail pressure and 0,32 ms pilot on-time, no EGR. The prediction accuracy of the off-line calibrated model is improved by its on-line adaptation.

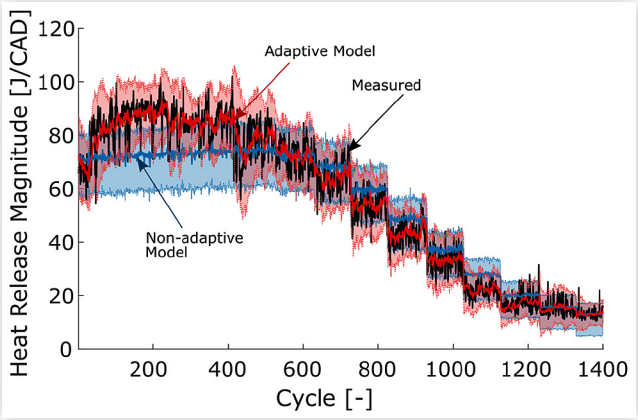

© 2019 Scania CV AB, Carlos Jorques Moreno, Ola Stenlåås, Per Tunestål.

More complex adaptation algorithm can be used for improved adaptation properties, such as a non-linear Kalman filter, but this is outside the scope of this paper.

Detection Threshold Adaptation

Another approach to improve the detection performance based on a cycle-to-cycle adaptation is to modify the detection threshold. The threshold γ is updated every cycle a diagnosis fails, proportionally to an adaptation gain K. For a faster update, the proposed recursive equation uses the additional information provided by the distance to the threshold:

$$\gamma_{n+1} = \gamma_n + K\frac{\delta_n - \hat{\delta}_n}{\varepsilon + |x_n - \gamma_n|} \tag{28}$$

$$\delta = \begin{cases} 1 & misfire \\ 0 & combustion \end{cases} \tag{29}$$

The result of the in-cycle misfire detection is $\hat{\delta}$ and the classification once the cycle is completed is δ. In this way, the threshold is not updated when the diagnosis is correct i.e. $\delta = \hat{\delta}$, but it is adjusted inversely proportional to the threshold distance when the in-cycle diagnosis fails. A small constant ε is added to avoid division by zero. Note that the sign of the correction is determined by the type of the diagnosis error.

© 2019 Scania CV AB, Carlos Jorques Moreno, Ola Stenlåås, Per Tunestål.

Sensor Fusion

Four variables have been used as indicators for the pilot misfire, the position of the pilot heat release magnitude, the pilot heat release magnitude, the accumulated heat release and the pressure rise over motoring. Each of these variables provides an indicator for the pilot misfire probability. Hence, by combining adequately these indicators, the detection performance can be increased.

It is desired to rely on those indicators that show the best detection performance. If no prior information is known about how accurate each indicator is, only the uncertainty from the calibration can be used to balance the fusion of the probability indicators. However, as done previously, the performance of each indicator can be evaluated on-line for an adaptive combination of them. The proposed combination is a weighted averaged of the predicted probabilities of misfire and combustion. The weights are updated proportionally to the successful ratio. As before, the distance to the threshold can be used as a measure of the indicator robustness i.e. how far from the threshold each probability is. The weights update is:

$$\omega_{n+1} = \omega_n + K\left(2\left(\delta_n - \hat{\delta}_n\right) - 1\right) \cdot \left| P\left(misfire | x_n\right) - P\left(fire | x_n\right) \right| \tag{30}$$

The weights are increased when the detection is successful i.e. $\delta = \hat{\delta}$ and decreased when it is not i.e. $\delta \neq \hat{\delta}$. Finally, the weights are normalized before computing the weighted average, in matrix form:

$$P_{combined,n} = \frac{\overrightarrow{\omega_n}}{\sum \omega_n} \times \left(\overrightarrow{P_n}\right)^{\mathrm{T}} \tag{31}$$

Results and Discussion

The results of the in-cycle pilot misfire detection are presented and discussed in this section. The in-cycle pilot misfire observability is first presented. The results of the in-cycle detector results are then introduced. It is followed by an analysis to understand the different performances of the algorithms, their sensitivity to errors and their limitations.

In-Cycle Pilot Misfire Observability

The results of the in-cycle pilot misfire observability using the measured and estimated variables are summarized in Table 5:

TABLE 5 In-cycle pilot misfire observability

	θ_{HR}	HR	AHR	ΔP	Combination
Diesel	93.93%	96.79%	96.80%	96.35%	98.10%
HVO	96.31%	98.37%	97.43%	97.41%	98.83%
RME	95.39%	97.86%	97.65%	97.27%	98.64%

© 2019 Scania CV AB, Carlos Jorques Moreno, Ola Stenlåås, Per Tunestål.

The maximum theoretical detection performance is given by the combined detection, which is about 98,5%. The remaining 1,5% of the cases cannot be correctly diagnosed in-cycle with any of the measured variables, even when all the information is available at any time.

The best observability is obtained for the magnitude of the heat release. The difference compared to the other variables is small, except for the CAD position of the heat release magnitude, with significantly lower observability i.e.-2,5%. The position of the pilot heat release magnitude will not be analyzed further on due to its poor performance compared to the other variables.

This result suggests that using any of the variables would give similar in-cycle pilot misfire performance. However, the performance and robustness of an in-cycle pilot misfire detector is associated with the dispersion of the optimal threshold i.e. the detection threshold must be as constant as possible for a robust diagnosis. This can be compared using the different coefficient of variation (COV), summarized in Table 6:

TABLE 6 Coefficient of variation of the optimal thresholds and combination

	θ_{HR}	HR	AHR	ΔP	Combination
Diesel	2.189	0.182	0.182	0.195	0.165
HVO	1.559	0.129	0.162	0.163	0.134
RME	1.459	0.148	0.155	0.168	0.140

© 2019 Scania CV AB, Carlos Jorques Moreno, Ola Stenlåås, Per Tunestål.

A lower coefficient of variation of the measurement variables indicates a more constant optimal detection threshold. The results show that the magnitude of the heat release will result in a more robust pilot misfire diagnosis. Nevertheless, the accumulated heat release has similar robustness. Again, the position of the pilot' heat release magnitude in the crank-angle domain has a wider dispersion, which will result in lower detection performance. The COV of the combination has a different interpretation. A lower coefficient of variation means that the detection by the measured variables is more consistent i.e. all measurement variables result in the same diagnosis.

To understand the effect of the different operating conditions on the pilot misfire observability, the theoretical maximum detection performance was computed for a sweep of the rail pressure, engine speed, pilot on-time, and SOI. The EGR had not a significant effect on the observability. It is hence omitted on the further analysis and discussion. The results are plotted in Figure 12:

The analysis of the trends in Figure 12 reveals that the most significant variables on the pilot misfire observability are the pilot on-time, start of injection and engine speed.

© 2019 Scania CV AB, Carlos Jorques Moreno, Ola Stenlåås, Per Tunestål.

FIGURE 12 Pilot misfire observability as a function of the operating variables, rail pressure, engine speed, injection on-time and start of injection. The sweep was done individually for each variable at the central point of 1200 bar rail pressure, 1200 RPM, no EGR. The fuel was conventional diesel. The effect of each individual variable on the observability is analyzed. The minimum is obtained at operating conditions with low signal-to-noise ratio, on the transition from pilot misfire to pilot combustion.

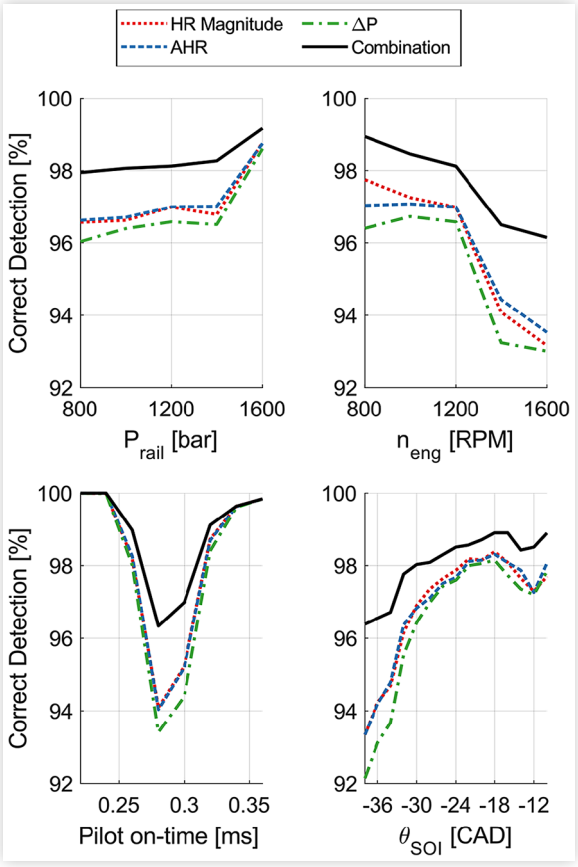

© 2019 Scania CV AB, Carlos Jorques Moreno, Ola Stenlåås, Per Tunestål.

The rail pressure has a less significant effect on the observability. The trend of the detection observability, expressed by the detection accuracy, is similar for all the measured variables.

The influence on the observability of the rail pressure and pilot on-time is explained by the resulting injected pilot mass. The minimum observability is obtained at the transition from misfire to combustion, which occurs at pilot masses about 10mg/st for these operating conditions. Higher rail pressure increases the injected pilot mass. Hence, it improves the observability due to the higher reactivity of the pilot fuel injection.

The cause for the effect of the SOI on the observability is the lower pilot reactivity at the lower in-cylinder pressure, which increases the ignition delay. The additional time enables the pilot fuel mass to mix with the air more homogeneously. The higher homogeneity reduces the combustion rate of the pilot, resulting in a lower heat release magnitude. The lower combustion rate reduces the signal-to-noise ratio of the measured signals, which reduces the observability.

A dip on the observability is observed at -12 CAD SOI. This effect is due to the additional oscillation of the HR trace for short pilot-main injection separations.

The effect of the engine speed on the observability is due to the additional turbulence and noise on the in-cylinder pressure signal. The oscillations on the signals have a higher amplitude, which decreases the signal-to-noise ratio. Hence, it is more difficult to distinguish between pilot combustion and oscillations, which reduces the misfire observability. Additionally, the higher engine speed reduces the ignition delay, which results in earlier pilot combustion. The lower charge density, due to the higher volume in the combustion chamber, reduces the heat release magnitude, resulting in a decreased observability.

Detection Performance

The detection performances of the algorithms are summarized in Figure 13 for the studied fuels:

FIGURE 13 Detection performances of the algorithms using the pressure rise over motoring, the heat release magnitude, the accumulated heat release and the combination of the three by sensor fusion, for the studied fuels. The calibration of the algorithms was optimized individually for each fuel. The relative detection performance of the different algorithms is compared.

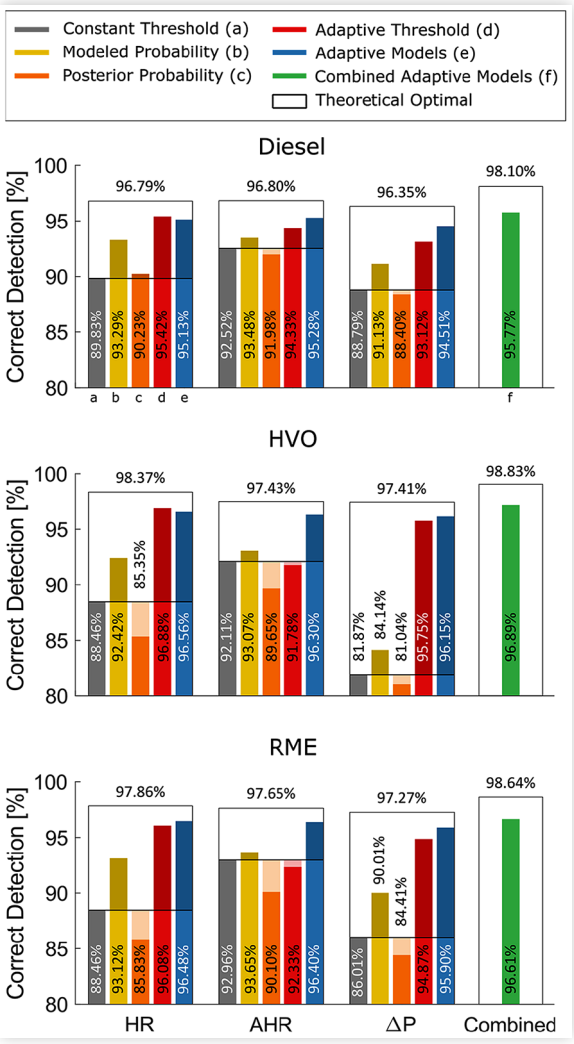

© 2019 Scania CV AB, Carlos Jorques Moreno, Ola Stenlåås, Per Tunestål.

© 2019 Scania CV AB, Carlos Jorques Moreno, Ola Stenlåås, Per Tunestål.

The measured variable that gives the best detection performance is the accumulated heat release. It has some disadvantages. It requires more computational resources than the pressure rise over motoring and more time than the magnitude of the heat release (an additional 2CAD are required to evaluate the AHR compared to the HR magnitude, see the discussion of the ignition delay model).

Analyzing the non-adaptive algorithms, using the constant calibrated detection threshold as the reference, the modeled posterior misfire probability improves the detection performance. The uncertainty of the predictive stochastic models makes the detection performance lower than using a simple threshold. The maximum detection performance with non-adaptive algorithms is at about 93.5% when using the AHR and the modeled posterior probability.

Evaluating the adaptive algorithms, the adaptation of the detection methods improves the detection performance significantly, which is brought close to the theoretical maximum. This is more apparent for the methods using the pressure rise used for HVO and RME, where the detection performance is increased up to a +15%. When using an adaptive threshold, the detection performance is improved up to +14% for the HVO using the pressure rise, and a minimum of +1.81% for the accumulated heat release using diesel, compared to a constant threshold detector. In general, the different measurement variables give similar results of the detection performance when the algorithms are adapted. This is evident for the adapted stochastic models' detector, which maximum difference between using the different measurement variables is 0.77%.

The adaptation increases the detection performance also compared to using any model for the detector design. The benefit of these methods is the reduced calibration effort. However, the exception of improved detection performance is found for the adaptive threshold detector using the AHR. Due to a too large gain for the feedback when using HVO and RME, the performance is lower than the constant threshold detector. The adaptation gain is therefore sensitive to the fuel and operating conditions for a good adaptation and detection performance. This inconvenience is not found for the stochastic models' adaptation, with a detection performance improvement of a +7% on average, with a minimum of +2.76% when using diesel, compared to the constant threshold detectors.

The sensor fusion of the adapted stochastic models further increases the detection performance, which gives the maximum detection performance on any of the fuels. However, the improvement is at about +0.5% on average compared to the best detector of each of the fuels.

Robustness Analysis

The in-cycle pilot misfire detection must be robust against the different operating conditions the engine runs. For the study of the detectors' robustness, the detection performance of the algorithm as function of the measured variables is plotted in Figure 14. Taking the theoretical optimal detection performance as the reference, the dip in the detection performance indicates the low signal-to-noise ratio as a function of the measured variable. The minimum is obtained at points where

FIGURE 14 Detection performance as a function of the variable used for detection, for the different algorithms. Conventional diesel fuel was used.

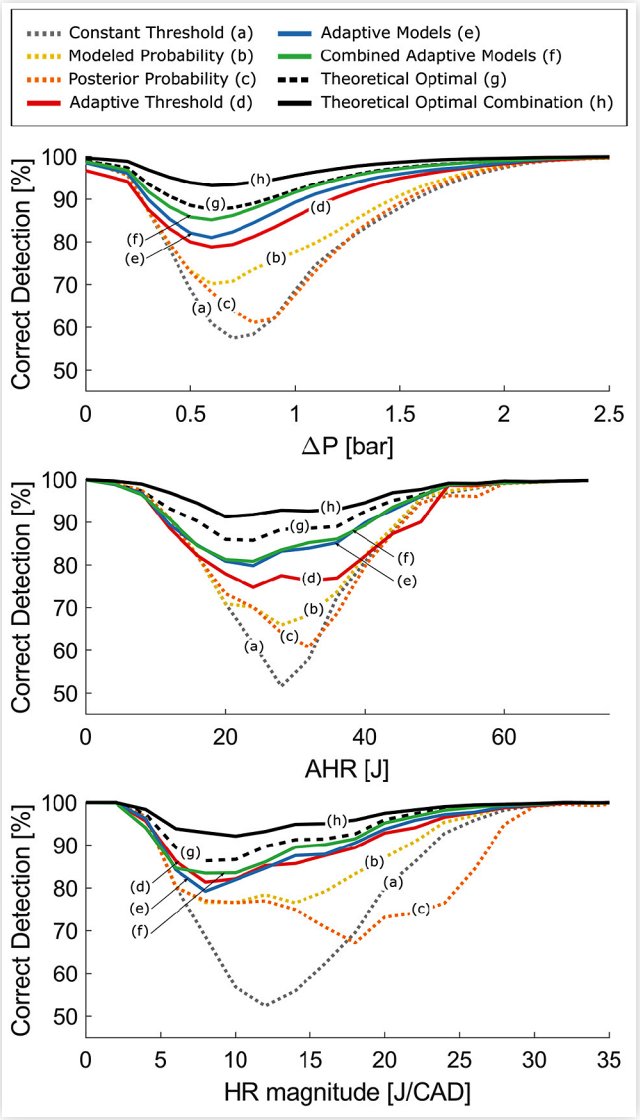

© 2019 Scania CV AB, Carlos Jorques Moreno, Ola Stenlåås, Per Tunestål.

the measured variable is similar to the noise of the signal, and hence it is difficult to distinguish between pilot combustion and pilot misfire. These cases are set by the different operating conditions, see Figure 12. High engine speeds, early pilot injections, low rail pressures, high EGR ratios and pilot on-times at the transition between pilot misfire and pilot combustion benefit these conditions.

The robustness of the different algorithms can also be compared using the results in Figure 14. The robustness of the modeled posterior probabilities is low due to the difficulty of having accurate predictive models in all operating conditions. It is, therefore, more robust to model the misfire probability directly as a function of the measured variable and operating conditions. However, if the methods are adaptive, the detection robustness is very similar between an adaptive threshold and an adaptive predictive model. The highest robustness is obtained in any case when the information is combined by sensor fusion.

© 2019 Scania CV AB, Carlos Jorques Moreno, Ola Stenlåås, Per Tunestål.

The robustness to the different combustion properties of the fuels was also studied. The calibration obtained for diesel for the in-cycle pilot misfire detection was used while running the engine with HVO and RME as fuels. The results are summarized in Figure 15, where the difference of each of the algorithms to their respective performance running diesel is plotted:

FIGURE 15 Robustness of the detection algorithms. The reference is the performance of the detectors calibrated for diesel. The higher robustness of the adaptive algorithms is compared to the non-adaptive algorithms.

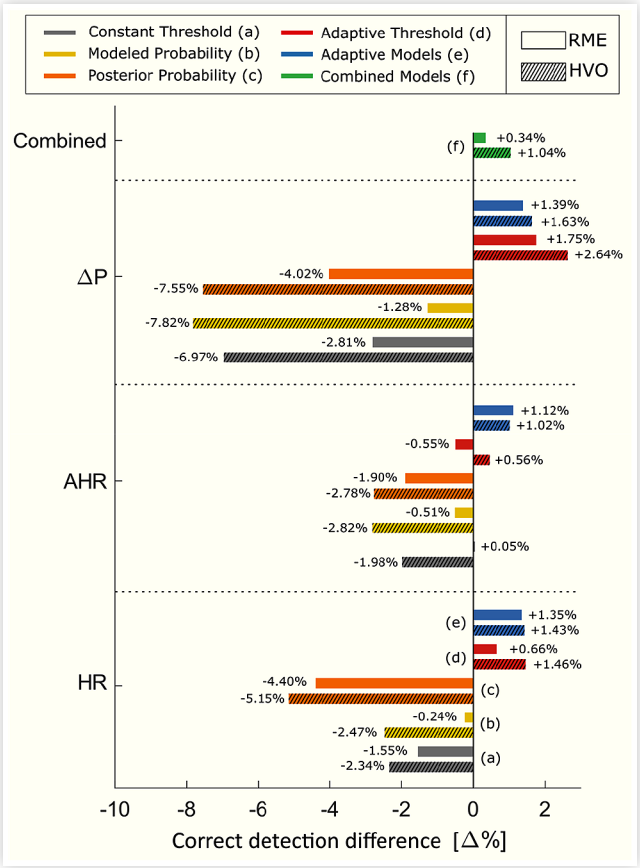

© 2019 Scania CV AB, Carlos Jorques Moreno, Ola Stenlåås, Per Tunestål.

Better robustness for the detectors with adaptive methods is observed. The methods based on previously calibrated models are the least robust (-3.4% on average), even less than using a constant threshold (-2.6% on average). On the other hand, if properly adapted, the methods based on calibrated models show the best robustness (+1.32% on average), similar to the detectors that use adaptive thresholds (+0.89% on average).

The differences must be interpreted relative to each other. The different results of the detection performance for the different fuels are due to the different signal-to-noise ratio of the signals when using each of the fuels.

Sensitivity Analysis

For the sensitivity analysis of each of the methods, the variables used as inputs in the models as well as the measured variables were modified with a constant offset. The resulting difference in the detection performance is plotted in Figure 16:

FIGURE 16 Sensitivity analysis of the detection methods to the measured variables. The highest sensitivity is obtained for errors on the variables used for the misfire detection, in comparison with the variables used as inputs in the predictive models.

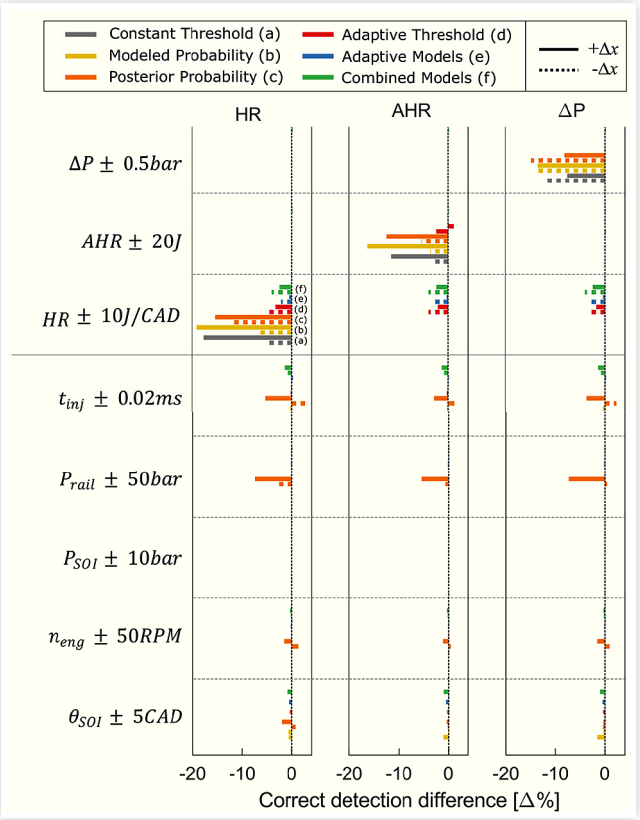

© 2019 Scania CV AB, Carlos Jorques Moreno, Ola Stenlåås, Per Tunestål.

The most sensitive method to input variables error is the detector based on the predictive stochastic models. The other methods can successfully overcome these input errors, either because they are not dependent on the input variables (for the constant threshold and direct posterior misfire probability-based detector) or because they can adjust to them (adapted threshold detectors and adapted stochastic models). Among the input variables, the injection on-time and rail pressure have the most significant effect. This is due to their effect on the estimated injected mass, used to compute the prior misfire probability, which off-sets the posterior probability, increasing the final detection error.

The non-adaptive methods are the most sensitive to errors on the measured variables. The error on the measured variable has the largest influence on the detectors based on that variable. The adaptive methods can overcome these disturbances

© 2019 Scania CV AB, Carlos Jorques Moreno, Ola Stenlåås, Per Tunestål.

successfully, but they show sensitivity to the measurement variables. The reason for the sensitivity is that the initial prediction error requires several cycles to adapt to the new measurements. Furthermore, the methods using the AHR or the pressure rise are also sensitive to measurement disturbances on the pilot HR magnitude. The error on the pilot HR magnitude is propagated to the adaptive methods using the AHR and the pressure rise. Contrary to what would be expected, the adaptive fusion of the detectors is more sensitive than the individual sensors. This is due to the disturbances generate erroneous feedback for the combination, resulting in increased sensitivity.

Conclusions

A comparison of different in-cycle pilot misfire detection algorithms is presented in this paper. Direct in-cylinder pressure measurement and variables estimated from it i.e. heat release and accumulated heat release are used for the misfire detection. Different techniques for in-cycle pilot misfire detectors design are presented, with and without cycle-to-cycle adaptation. For the non-adaptive methods, a constant calibrated threshold, a modeled misfire probability as a function of the operating conditions, and a posterior misfire probability (computed through the Bayes theorem from predictive stochastic models) have been used. For the adaptive methods, an adaptive threshold, an adaptation of the predictive models and adaptive combination of the posterior probabilities as a sensor fusion technique, have been used. The results are compared to the theoretical maximum in-cycle pilot detection performance that can be obtained i.e. in-cycle pilot misfire observability. The robustness of the different algorithms to the operating conditions and the sensitivity analysis of the algorithms have been discussed.

A Scania D13 modified engine has been used to collect the data and test the algorithms at different engine speeds, rail pressures, EGR levels, pilot start of injection and on-times, using conventional diesel, HVO, and RME as fuels. The results show that for the non-adaptive algorithms, using the heat release magnitude and accumulated heat release gave similar detection performance (around 90% correct detection ratio on average). The advantage of using the heat release magnitude is a faster diagnosis and less use of computational resources. However, it is less robust than using the accumulated heat release (+1% detection error). The reliance of the predictive stochastic models on an accurate calibration results in a lower detection performance than the modeled probability detector (-3% correct detection). This issue is overcome by the models' adaptation.

The adaptive methods have better detection performance and are significantly more robust against operating conditions and fuel. The adaptive threshold detector gave similar results as using the adaptive predictive stochastic models' detector (around 95% correct detection ratio on average). The advantage is less computational resources and calibration. However, care must be taken when calibrating the feedback gain. The main disadvantage is that the adaptation can only be done when there are incorrectly diagnosed cycles. In this respect, the adaptive predictive stochastic detector can use the information of every cycle, increasing the detector performance and robustness. The information used in the detectors can easily be combined, resulting in the best detection performance and robustness. Due to the cycle-to-cycle feedback, the adaptive methods are more sensitive to measurement errors, being the errors on the heat release magnitude the most significant ones (+15% detection error for the non-adaptive and -3% for the adaptive detectors, with a bias of +10 J/CAD).

As a general conclusion, adaptation is required for a robust in-cycle pilot misfire diagnosis. The adaptive threshold detector using the heat release magnitude has a good compromise between detection performance, robustness, early detection, and low sensitivity if the feedback gain is calibrated adequately. The use of the adapted predictive stochastic detectors, using sensor fusion, can only be motivated if higher detection performance is required.

The limitations of the methods are directly related to the signal-to-noise ratio of the measured signals. At some operating points, the correlation of the signals and pilot misfire is too powerless to detect the pilot misfire. To overcome these limitations, additional measured variables can be used and combined, such as the use of knock sensor. Despite the good performance of the adaptive algorithms, more complex adaptation and sensor fusion techniques can further improve the detection performance.

References

1. Jorques Moreno, C., Stenlåås, O., and Tunestål, P., "Investigation of Small Pilot Combustion in a Heavy-Duty Diesel Engine," *SAE Int. J. Engines* 10(3):1193-1203, 2017, doi:10.4271/2017-01-0718.
2. Jorques Moreno, C., Stenlåås, O., and Tunestål, P., "Influence of Small Pilot on Main Injection in a Heavy-Duty Diesel Engine," SAE Techcnical Paper 2017-1-708, 2017, doi:10.4271/2017-01-0708.
3. Turesson, G., *Model-Based Optimization of Combustion-Engine Control* (Lund University, 2018). ISBN:9789177537052.
4. Jorques Moreno, C., Stenlåås, O., and Tunestål, P., "In-Cycle Closed-Loop Combustion Control with Pilot-Main Injections for Maximum Indicated Efficiency," *IFAC-PapersOnLine* 51(31):92-98, 2018.
5. The Air Resources Board (ARB), "Heavy-Duty On-Board Diagnosis Legislation," 2013.
6. Mohammadpour, J., Franchek, M., and Grigoriadis, K., "A Survey on Diagnostic Methods for Automotive Engines," *Int. J. Engine Res.* 13(1):41-64, 2012, doi:10.1177/1468087411422851.

© 2019 Scania CV AB, Carlos Jorques Moreno, Ola Stenlåås, Per Tunestål.

7. Kiencke, U., "Engine Misfire Detection," *IFAC Proc.* 30(18):645-650, 1997, doi:10.1016/S1474-6670(17)42473-6.
8. Connolly, F. T. and Rizzoni, G., "Real Time Estimation of Engine Torque for the Detection of Engine Misfires," *J. Dyn. Syst. Meas. Control* 116(4):675, 1994, doi:10.1115/1.2899267.
9. Eriksson, D., Eriksson, L., Frisk, E., and Krysander, M., "Flywheel Angular Velocity Model for Misfire and Driveline Disturbance Simulation," *IFAC Proc.* 46(21):570-575, 2013, doi:10.3182/20130904-4-JP-2042.00020.
10. Jung, D., Eriksson, L., Frisk, E., and Krysander, M., "Development of Misfire Detection Algorithm Using Quantitative FDI Performance Analysis," Feb. 2019, doi:10.1016/j.conengprac.2014.10.001.
11. Zhang, Y., Zhou, T., Zheng, T., Han, W., Tan, R., and Wang, Y., "Misfire Detection Based on Switched State Observer of Hybrid System in Internal Combustion Engine," in *AIP Conference Proceedings*, AIP Publishing LLC: 020043, 2017, doi:10.1063/1.4979775.
12. Lindemann, M. and Filbert, D., "Methods of Misfire Detection Using Knock Sensors," *MTZ Worldw.* 63(3):16-18, 2002, doi:10.1007/BF03227529.
13. Chang, J., Kim, M., and Min, K., "Detection of Misfire and Knock in Spark Ignition Engines by Wavelet Transform of Engine Block Vibration Signals," *Meas. Sci. Technol.* 13(7):319, 2002, doi:10.1088/0957-0233/13/7/319.
14. Singh, S., Potala, S., and Mohanty, A. R., "An Improved Method of Detecting Engine Misfire by Sound Quality Metrics of Radiated Sound," *Proc. Inst. Mech. Eng. Part D J. Automob. Eng.* 095440701881869, 2018, doi:10.1177/0954407018818693.
15. Villarino, R. and Bohme, J. F., "Pressure Reconstruction and Misfire Detection from Multichannel Structure-Borne Sound," *2004 IEEE International Conference on Acoustics, Speech, and Signal Processing*, IEEE, ISBN 0-7803-8484-9, ii-141-4, Feb. 2019, doi:10.1109/ICASSP.2004.1326214.
16. Fan, Q., Bian, J., Lu, H., Tong, S., and Li, L., "Misfire Detection and Re-Ignition Control by Ion Current Signal Feedback during Cold Start in Two-Stage Direct-Injection Engines," *Int. J. Engine Res.* 15(1):37-47, 2014, doi:10.1177/1468087412458099.
17. Auzins, J., Johansson, H., and Nytomt, J., "Ion-Gap Sense in Misfire Detection, Knock and Engine Control," *SAE Trans.* 104:1-8, 1995, doi:10.2307/44633194.
18. Helm, S., Kozek, M., and Jakubek, S., "Combustion Torque Estimation and Misfire Detection for Calibration of Combustion Engines by Parametric Kalman Filtering," *IEEE Trans. Ind. Electron.* 59(11):4326-4337, 2012, doi:10.1109/TIE.2012.2193855.
19. Cesario, N., Tagliatatela, F., and Lavorgna, M., "Methodology for Misfire and Partial Burning Diagnosis in SI Engines," *IFAC Proc.* 39(16):1024-1028, 2006, doi:10.3182/20060912-3-DE-2911.00176.
20. Glavmo, M., Spadafora, P., and Bosch, R., "Closed Loop Start of Combustion Control Utilizing Ionization Sensing in a Diesel Engine," SAE Technical Paper 1999-01-0549, 1999, doi:10.4271/1999-01-0549.

Contact Information

carlos.jorques@scania.com

Acknowledgments

The authors acknowledge the Swedish Energy Agency for funding this research project, the Competence Center for the Combustion Processes (KCFP) at Lund University, LTH and Scania CV AB for the test equipment facilities. The technicians at the Lund University lab are acknowledge for their valuable assistance. The NCP group at Scania is acknowledge for their support while working with the rail pressure signal.

Definitions/Abbreviations

AHR - Accumulated Heat Release
ATDC - After Top Dead Center
CAD - Crank Angle Degree
CARB - California Air Resources Board
CLCC - Close-Loop Combustion Control
COV - Coefficient of Variance
ID - Ignition Delay
EGR - Exhaust Gas Recirculation
EVO - Exhaust Valve Open
FPGA - Field Programmable Gate Array
HR - Heat Release
HVO - Hydrogenated Vegetable Oil
IVC - Inlet Valve Closing
OBD - On-Board Diagnostics
RME - Rapeseed Methyl Esters
RPM - Revolutions per Minute
SOC - Start of combustion
SOI - Start of injection
TDC - Top Dead Center

Symbols

P - Probability
N - Normal distribution
$\boldsymbol{x}$ - Generic input variable
$\boldsymbol{\tau}$ - Time delay
$\boldsymbol{f}$ - Generic model function
$\boldsymbol{\theta}$ - Crank angle degree (CAD)
$\boldsymbol{\sigma}$ - Standard Deviation
$\boldsymbol{q}$ - Heat release rate
$\boldsymbol{Q}$ - Heat release
$\boldsymbol{w}$ - Weight
$\boldsymbol{u}$ - Generic input vector

© 2019 Scania CV AB, Carlos Jorques Moreno, Ola Stenlåås, Per Tunestål.

Δ - Change in a variable
K - Gain constant
k - Parametrization constant
α - Forgetting factor
δ - Boolean misfire variable
γ - Detection threshold
ε - Small value
$\mathbf{e}$ - error

Lower index

$\mathbf{n}$ - Cycle index

Upper index

$\hat{}$ - Estimated variable
$\bar{}$ - Normalized variable
^{T} - Transpose

© 2019 Scania CV AB, Carlos Jorques Moreno, Ola Stenlåås, Per Tunestål. Published by SAE International. This Open Access article is published under the terms of the Creative Commons Attribution License (http://creativecommons.org/licenses/by/4.0/), which permits distribution, and reproduction in any medium, provided that the original author(s) and the source are credited.

Positions and opinions advanced in this work are those of the author(s) and not necessarily those of SAE International. Responsibility for the content of the work lies solely with the author(s).

e-ISSN 2641-9645